

# Pore structure and surface acidity evaluation of Fe-PILCs

Suna BALCI\*, Elif GÖKÇAY

*Gazi University, Engineering and Architecture Faculty, Chemical Engineering Department  
06570 Maltepe-Ankara TURKEY  
e-mail : sunabalci@gazi.edu.tr*

Received 29.07.2008

Fe-PILCs via different conditions using smectites from Hancili (Turkey) and Wyoming (USA) were synthesised. Presaturation had little effects on the basal spacing values while it had important effects on thermal stabilities of the products. Products having basal spacing ( $d_{001}$ ) around 1.30 nm and surface area up to  $160 \text{ m}^2 \text{ g}^{-1}$  were obtained. The thermal behaviour, X-ray diffraction (XRD) patterns, and nitrogen adsorption/desorption experiments confirmed that thermally stable and micro-mesoporous products were obtained although at elevated calcination temperature. Delaminated sample with basal spacing value of 2.79 nm was obtained. Surface acidity of clay was enhanced by pillaring. Chemically sorbed pyridine Fourier transform infrared spectroscopy (FTIR) bands were preserved at elevated desorption temperatures.

**Key Words:** Pillared clays, delaminated clays, characterisation, surface area, surface acidity.

## Introduction

Smectites, expandable layered alumina/magnesia-silicates, are important materials with a large variety of applications in the chemical industry as adsorbents and catalyst supports. In these applications permanent high porosity and molecular sieve properties are the desired properties. The concept of pillaring is very straightforward; intercalation (by ion exchange) and fixation (by calcination) of bulky molecules keep the layers of the smectite clays apart, resulting in pillared intercalated layered clays (PILCs). Moreover, as access to the interior pore volumes of pillared clays is controlled by the distance between the silicate layers and the distance between the pillars, one or both distances may be adjusted to suit a particular application choosing the right pillar agent. The desired product must have permanent molecular sieve properties with the desired

---

\*Corresponding author

pore dimensions and good thermal and hydrothermal stabilities. Firstly, the intercalation of clays was studied using organic compounds.<sup>1</sup> Due to the lack of thermal stability of the pillared layered clays obtained from organic compounds, later studies were orientated towards the use of inorganic compounds. Literature studies have shown that the use of inorganic metal oxides or salts, which form polynuclear species upon hydrolysis as pillar agents, provides thermally stable pillared clays with high surface areas.<sup>2–5</sup> The pillared clays have both Brönsted and Lewis acid sites, which give them catalytic properties. During the dehydroxylation of the pillars, Brönsted acidity could be combined with the liberation of protons. It decreases markedly with increasing calcination temperature, by either dehydroxylation of surface or by migration of protons from the interlayer space into the octahedral sheet. High temperature treatments of pillared montmorillonites have caused decreases in the numbers of both acid sites, supporting the second explanation.<sup>2–4,6–10</sup>

Several studies have been reported in the literature using iron as the pillar agents' source. Fe-PILCs show magnetic and high catalytic activity.<sup>4,5,11–17</sup> The disadvantage of Fe-PILCs is the resulting small basal spacing. However, in some works,<sup>18–23</sup> delaminated structured Fe-PILCs with basal spacing values higher than 1.4 nm at room temperature were obtained, and upon calcination decreases in d-spacing occurred. In the present study Fe-PILCs were synthesised and their structural and thermal properties and surface acidities were investigated.

## Experimental

A bentonite sample from the Hançili region, which is a small town in Central Anatolia, (named Hançili Green Bentonite (HGB) according to its appearance) was the main clay used. The well-known SWy-2 (Na-Wyoming montmorillonite), which is considered a standard clay, was also used as host matrix for the synthesis of PILCs. The effects of preparation techniques on the surface properties of PILCs were investigated.<sup>24</sup>

### Preparation of the host mineral

In the synthesis of PILCs, the natural and pre-saturated clay samples with particle sizes less than 200 mesh were used. For the pre-saturation 1 g air-dried samples were treated with 5 mL solutions of sodium and calcium sources (NaCl, CaCl<sub>2</sub> with 1 M concentration) for several hours. The slurry was then centrifuged at -4 °C with a Sanyo Mistral 2000 Model Centrifuge, and the solid particles were washed with demineralised water several times to get rid of excess sodium/calcium ions. The synthesis of Fe-PILCs was carried out by making good use of the recipe used by Maes and Vansant.<sup>25</sup> The effects of pre-saturation type, pillar solution synthesis conditions, ion exchange step, and calcination temperature on the product quality were investigated.

### Fe-PILCs synthesis

The salt of ferric chlorine was used in Fe-PILCs synthesis. The excess acidity of the starting solution, which was 0.2 M FeCl<sub>3</sub>.6H<sub>2</sub>O solution, was removed by adding Na<sub>2</sub>CO<sub>3</sub> powders requiring an OH/Fe molar ratio of 2.0. The hydrolysis was carried out at room temperature for 16 h under continuous stirring. Clay powders were added gradually to pillar solution proving 6.5 mmol Fe per gram of clay. Pillar agent-clay suspensions were stirred for 3 h at room temperature to allow ion exchange between exchangeable cations of the clay and

pillar precursors. The formed PILCs were centrifuged, washed, dried in air, and calcined in air at different temperatures for 3 h. The effects of pre-saturation were investigated.

## Characterisation studies

SEM photograph of the HGB bentonite was taken by Jeol JSM-840 A Scanning Electron Microscope. The chemical analysis of the host samples was performed with an X'Cem Model X-Ray Fluorescence Spectrometer. Sodium saturation was used to measure the cation exchange capacities (CECs) of the host samples.<sup>26</sup> Thermal behaviour of the HG bentonite was investigated by Linseis L 81 TGA under 12.00 L h<sup>-1</sup> nitrogen flows with a heating rate of 5 °C min<sup>-1</sup>.

Single point surface area values of the samples (PILCs) were measured by nitrogen adsorption at 77 K under continuous flow of 30 vol.% nitrogen-70 vol.% helium mixture using a Quantachrome Monosorb Direct Surface Analyser. Their solid densities were determined by means of a Micromeritics 1305 Model He-air Pycnometer. X-ray diffraction patterns of the samples were recorded by means of a Philips PW 3710 Model X-Ray Diffractometer with Cu K $\alpha$  radiation.

For the sample synthesised from 1 day Na-saturated HGB clay, detailed characterisation studies were carried out. The thermal behaviour of these samples (host and the pillared product) was investigated under the same conditions used for HGB bentonite. SEM photographs of them were taken again using a Jeol JSM-840 A Scanning Electron Microscope. Nitrogen adsorption/desorption isotherms of Fe-PILC were obtained at 77 K by means of a Quantachrome Autosorp 1C model. Before the measurements, the samples were degassed at 573 K for 2 h under vacuum. To get an idea about the delamination of the structure X-ray diffraction patterns of the Fe-PILC were recorded by means of a Philips Expert PW 3070, which enables the detection of the peaks above  $2\theta$  values of 1.0° with Cu K $\alpha$  radiation. Total surface acidities of HB bentonite and Fe-PILC were determined by volumetric titration.<sup>27</sup> In this method, the dried samples were saturated with NaOH in a short time and then they were titrated with H<sub>2</sub>SO<sub>4</sub>. Acidity was described as milliequivalents of base used per 100 g of dried solid. Infrared spectra of the same samples with and without the pyridine adsorption were obtained using KBr pellets on an Ati Unicam Mattson 1000 FTIR spectrometer. Pellets were prepared by mixing 1 mg of sample with 100 mg of KBr. FTIR spectra of pyridine adsorbed then desorbed at room temperature, 150, 250, and 350 °C samples were recorded to get an idea about the type/distribution of acid sites.

## Results and discussion

### Characterisation of Hançılı Bentonite

Hançılı Green Bentonite (HGB) had a honeycomb structure similar to other bentonite type rocks (Figure 1a). The chemical analysis and some mineralogical properties of HGB<sup>28,29</sup> were similar to those of well-known SWy-2 montmorillonite (Table 1). The presence of a high amount of iron (6.11% Fe<sub>2</sub>O<sub>3</sub>) in the structure gave the greenish appearance to the Hançılı bentonite. The chemical analysis showed that both minerals had SiO<sub>2</sub> content higher than that of the montmorillonite (>55%). This increase was due to the presence of impurities. XRD patterns (Figure 1b) showed a great intensity at  $2\theta \cong 26.6^\circ$ , the diffraction of (101) arising from the quartz impurity.<sup>30,31</sup> Moreover, one of the main peaks of montmorillonite also gave high intensity at  $2\theta \cong 26.6$ .

Dolomite and feldspar were also found as impurities. From the XRD patterns, the (001) basal reflection values (which are the characteristics of the condition, i.e. interlayer water and exchangeable cations) were determined as 1.25 nm and 1.24 nm at room temperature for SWy-2 and HGB samples, respectively, confirming that they were in their Na<sup>+</sup> exchanged forms. On ethylene glycol swelling, an increase in (001) reflection of around 0.4 nm was observed. The peak that occurred at  $2\theta \cong 19.9^\circ$  was 2-dimensional 02 and 11 bands (which are the characteristics of the type of clay mineral) arising from the random stacking of layers. The small peak that occurred at  $2\theta \cong 34.9^\circ$  was also one of the major peaks assigned to the 2-dimensional diffraction, *hk*, reflections (Figure 1b).<sup>11,30–31</sup> An increase in temperature to 300 °C caused decreases in basal spacing values due to the moisture removal between the clay sheets (Figure 1b, Table 1). This behaviour was in good agreement with the thermal behaviour (Figure 2). TGA data showed a high mass loss rate up to 150 °C. Between 200 and 450 °C dehydration occurred and the decomposition of clay mineral itself started above 600 °C.<sup>24,30–32</sup>

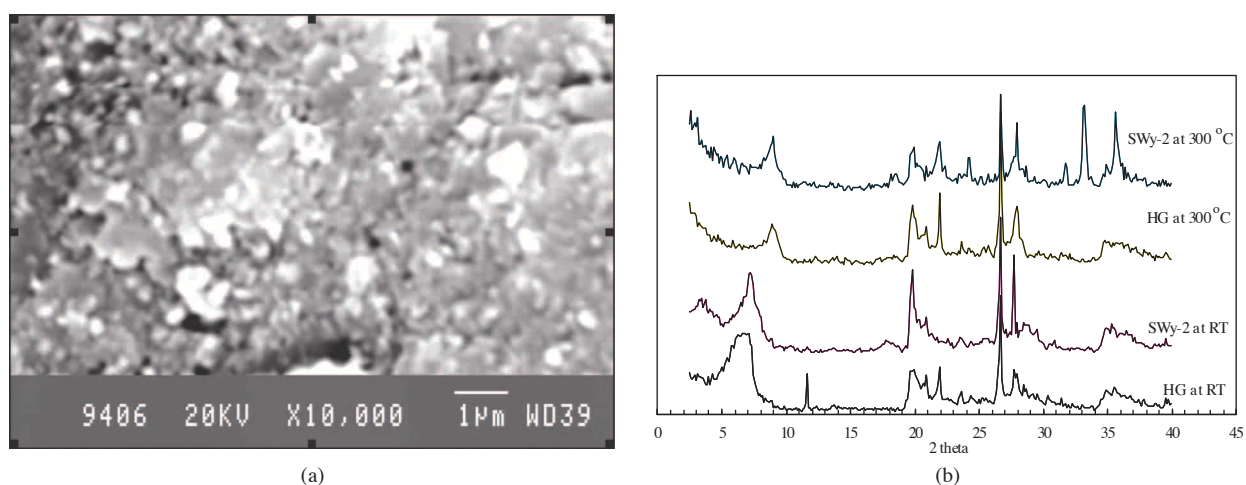


**Figure 1.** (a) SEM image of HGB (b) XRD patterns of HGB<sup>29</sup> and SWy-2 at room temperature (RT) and 300 °C.

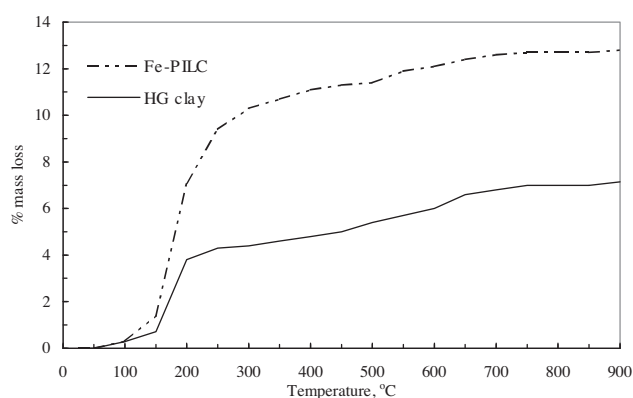


**Figure 2.** Thermal behaviours of HGB and Fe-PILC (heating rate = 5 °C (min)<sup>-1</sup>; nitrogen flow rate = 12 L h<sup>-1</sup>).

**Table 1.** Physicochemical and structural properties of the samples used.

metal oxides, mass %	HG <sup>27</sup>	SWy-2
SiO <sub>2</sub>	66.95	68.58
Al <sub>2</sub> O <sub>3</sub>	18.38	20.56
Fe <sub>2</sub> O <sub>3</sub>	6.11	4.25
MgO	2.76	2.71
CaO	1.80	1.74
Na <sub>2</sub> O	2.81	1.49
K <sub>2</sub> O	1.19	0.67
d-spacing, (d <sub>001</sub> ) nm (room temp.)	1.24	1.25
d-spacing, (d <sub>001</sub> ) nm (300 °C)	9.83	9.83
solid density ( $\rho_s$ )g cm <sup>-3</sup> (100 °C)	2.54	2.57
C.E.C., meqv.(100g) <sup>-1</sup>	50	66
surface acidity, meqv.(100g) <sup>-1</sup>	46	

## Fe-PILCs

**Effect of pre-saturation on the quality of Fe-PILCs:** The synthesis conditions and the effects of the pre-saturation process on Fe-PILCs are summarised in Table 2 and their XRD patterns are given in Figure 3. The different pH values obtained after the ion-exchange period, although using the same pillar solution, confirmed that the pre-saturation had some effects on the degree of ion exchange and interpillar spacing values. At 100 °C, d<sub>001</sub> values of the samples obtained from SWy-2 and 1-week Na-saturated HGB sample were 1.23 nm and 1.25 nm, respectively. Slightly higher values were obtained for the samples synthesised from 1-day Na-saturated HGB and Ca-saturated SWy-2 clays (1.31 nm and 1.29 nm, respectively), due to the arrangement of pillar agents between the clay sheets and the left exchangeable ions. The uniform pillared structured product showing high XRD peak intensity at (001) reflection was obtained from SWy-2, while a small deformation in the pillared structure occurred with its pre-saturation. Ca-saturation and dual pre-saturation (Na<sup>+</sup> saturation followed by Ca<sup>2+</sup> saturation) resulted in decreases in surface area values. The increase in pre-saturation time might bring about the uniform distribution of the pillar agents within the sheets of HGB. Hence the highest peak intensity was observed for the sample obtained from 1-week Na-saturated HGB sample. On calcination at 800 °C nearly the same d<sub>001</sub> and surface area values were achieved independent of pre-saturation type as expected. Small decreases in the XRD peak intensities were observed with the increase in calcination temperature. The uniform distribution of the pillar agents within the structure should yield high thermal stability and so PILCs from 1 week Na-saturated HGB preserved their structure at high calcination temperature. Dual pre-saturation of HGB gave samples with lower XRD peak intensity compared with the others; however, the strength of the intensity was preserved at 800 °C calcination (Table 2, Figure 3).

During the ion exchange, pH values of pillar agent-clay suspension were below 2.0. At low pH values (lower than 3.0) most of the surface sites could be occupied by hydrogen ions.<sup>33</sup> This might limit the entrance of more pillars into the structure, and so interpillar distance could be arranged high. For the pores in the micropore ranges, this phenomenon could result in products with high surface areas.<sup>24</sup> The surface area values

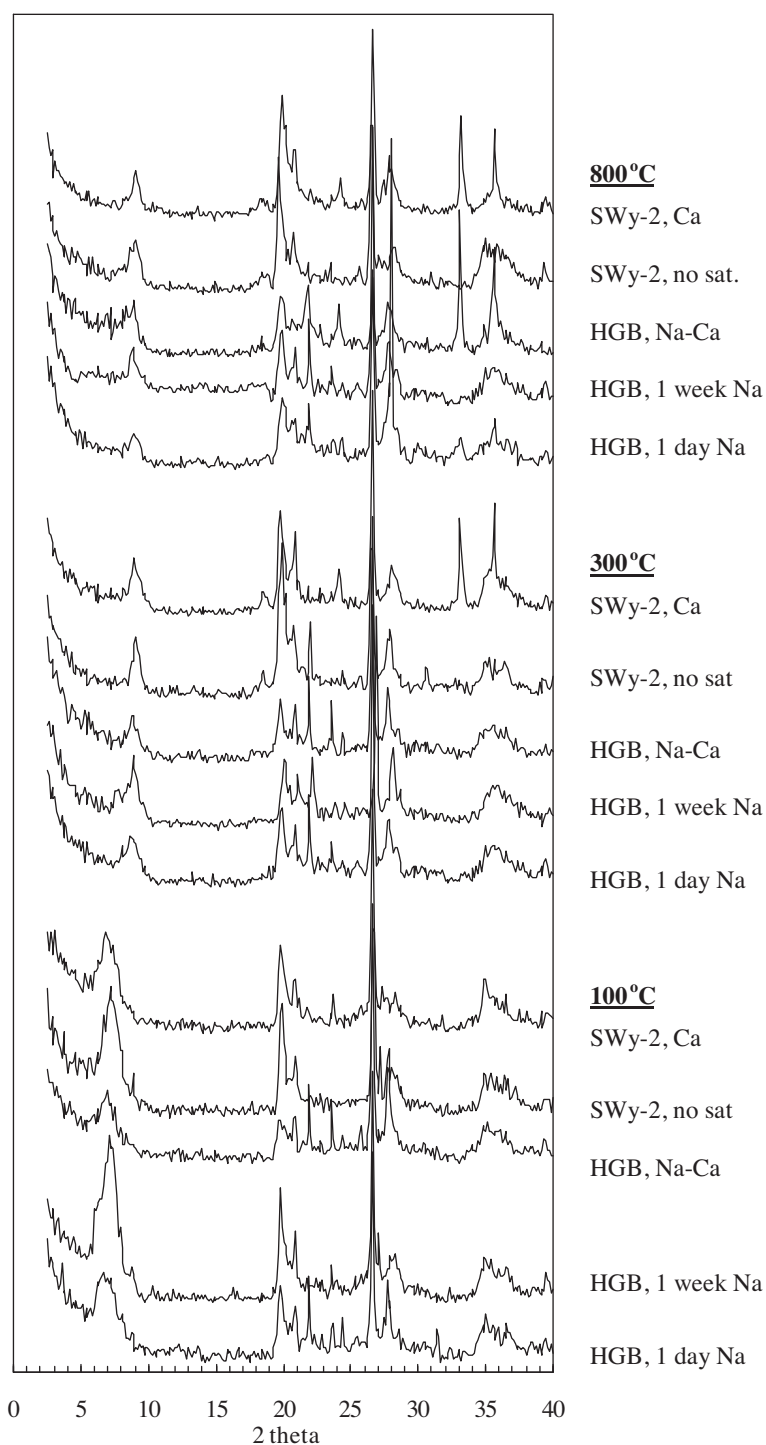


**Figure 3.** XRD patterns of Fe-PILCs obtained via different pre-saturation types at different calcination temperatures.

of the PILCs obtained from SWy-2 mineral were lower than those of the others at all calcination temperatures. The standard clay mineral had a cation exchange capacity of  $66 \text{ meqv.}(100 \text{ g})^{-1}$ , which was higher than that of HGB (Table 1). Therefore, in the ion exchange step more pillars could be taken by this mineral. This

**Table 2.** Effect of pre-saturation of clay on Fe-PILCs quality.

Host clay and pre-saturation type	pH of the pillar-clay suspension before ion exchange	pH of the pillar-clay suspension after ion exchange	100 °C			300 °C			650 °C			800 °C		
			d <sub>001</sub> <sup>*</sup> (nm)	S <sub>s.p.</sub> <sup>**</sup> (m <sup>2</sup> g <sup>-1</sup> )	d <sub>001</sub> (nm)	ρ <sub>s</sub> <sup>***</sup> (g cm <sup>-3</sup> )	S <sub>s.p.</sub> (m <sup>2</sup> g <sup>-1</sup> )	ρ <sub>s</sub> (g cm <sup>-3</sup> )	S <sub>s.p.</sub> (m <sup>2</sup> g <sup>-1</sup> )	d <sub>001</sub> (nm)	ρ <sub>s</sub> (g cm <sup>-3</sup> )	S <sub>s.p.</sub> (m <sup>2</sup> g <sup>-1</sup> )	d <sub>001</sub> (nm)	ρ <sub>s</sub> (g cm <sup>-3</sup> )
HGB-NaCl (1 day pre-saturation)	1.76	1.70	1.31	102.3	1.02	2.61	86.9	2.64	65.8	1.00	2.76			
HGB-NaCl (1 week pre-saturation)	1.76	1.57	1.25	114.0	1.03	2.99	73.5	2.77	65.9	0.99	2.79			
HGB-NaCl/CaCl <sub>2</sub> (dual pre-saturation)	1.76	1.57	1.27	111.2	1.01	2.80	74.7	2.52	66.7	0.99	2.42			
SWy-2 (without pre-saturation)	1.82	1.66	1.23	84.9	0.98	3.04	56.2	2.48	56.0	0.97	2.63			
SWy-2 (Ca pre-saturation)	1.81	1.72	1.29	49.9	0.98	2.89	47.2	2.72	41.1	0.97	2.66			

\* basal spacing  
 \*\* single point surface area  
 \*\*\* solid density

phenomenon resulted in a product with good molecular sieve properties although it might cause decreases in basal spacing, interpillar spacing, and surface area values. XRD patterns showed high peak intensity, confirming the uniform distribution of pillars. Ca-saturation of SWy-2 let the structure take more pillar ions. Therefore, the surface area at 300 °C was nearly halved by the calcination at higher temperatures due to the hydroxylation of the pillar agents (Table 2). Furthermore, the spreading out behaviour of the XRD pattern also confirmed the nonuniform distribution of pillar agents (broad peak intensity was observed). It was seen that, other than the (001) plane, reflections were preserved by pillaring (Figure 3). The decreases in solid density values were observed because of the removal of the structural water up to 600 °C; then slight increases occurred due to the layer deformation. Decreases in surface area values and increases in solid density values were low above 650 °C calcination temperature. For the rest of the study, 1 day NaCl presaturated bentonite was used as the host.

**Thermal behaviour:** Thermal behaviour of Fe-PILC is seen in Figure 2. Around 1.8% mass losses occurred with drying up to 150 °C. Interlayer water removal caused approximately 10% of total mass loss up to 250 °C. Pillar precursors deformed in the clay and corresponding loss of OH groups occurred up to 500 °C with small mass losses and dehydration of pillars above 500 °C. At elevated temperatures the effect of calcination temperature on the product quality might be evident.

**Textural properties:** SEM photograph of Fe-PILC is seen in Figure 4. The firm packed form of the original clay (Figure 1a) was destroyed by the pillaring yielding porous material. Flake formation was observed. Nitrogen adsorption/desorption isotherms of Fe-PILC are also seen in Figure 5. The adsorption isotherm gave small plateaus at around 32 cm<sup>3</sup> g<sup>-1</sup> gas adsorption volume. The isotherms showed hysteresis loops in the desorption branch, indicating the presence of some amount of mesopores resembling type IV isotherm of BDDT classifications with a well-defined H4 hysteresis loop. This behaviour was the indication of a mono-multilayer adsorption on slit-shaped pores among plate-like particles.<sup>34</sup> The opening behaviour of the hysteresis loop indicated the formation of irregular shape pores. The opening in hysteresis loop that occurred for Fe-PILC demonstrated the presence of mesopores in the pillared structure. These behaviours were also observed in SEM photographs (Figures 1 and 4). Multi-point BET and Langmuir surface area values were 96.3 and 142.7 m<sup>2</sup> g<sup>-1</sup>, respectively. Multi-point surface area value was comparable with the one calculated from the single point

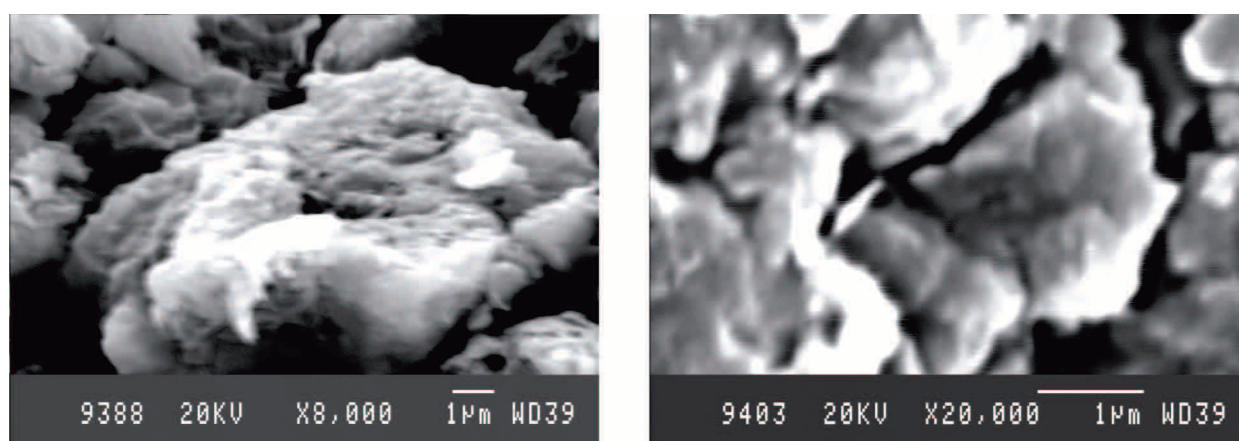


**Figure 4.** SEM images of Fe-PILC.

nitrogen adsorption experiment, while the Langmuir isotherm fit gave the highest surface area value (Table 3). Total meso- and micropore volume values estimated from the desorption value at 0.96 and 0.01 relative pressure were 0.0799 and 0.0235 cm<sup>3</sup> g<sup>-1</sup> while the micropore volume value estimated from t-plots was 0.0097 cm<sup>3</sup> g<sup>-1</sup>.

**Table 3.** Some structural properties of Fe-PILC synthesised from 1 week Na-saturated HGB and calcined at 300 °C.

Surface area, m <sup>2</sup> g <sup>-1</sup>			Pore volume, cm <sup>3</sup> g <sup>-1</sup>				Basal spacing	Volumetric titration
single point, S <sub>sp.</sub>	multipoint BET, S <sub>BET</sub>	Langmuir, S <sub>L</sub>	monolayer, V <sub>m</sub> , (from BET)	monolayer, V <sub>m</sub> , (from Lang.)	micropore, V <sub>micro</sub> , (from t-plot)	meso+micro, V <sub>meso+micro</sub> , (at 0.96 P/P <sub>0</sub> desorption)	d <sub>001</sub> (nm)	surface acidity, meqv.(100 g) <sup>-1</sup>
102.3	96.3	142.7	0.0343	0.0505	0.0097	0.0799	2.79	127.93

The XRD patterns showed 3 main peaks for 2θ values of lower than 10° (Figure 6). It could be said that the pillaring procedure also caused the delamination of the structure. The high intensity peaks occurred at 2θ of 6.60° (d<sub>001</sub> = 1.34 nm) and 2θ = 3.17° (d<sub>001</sub> = 2.79 nm) and a rather small peak occurred at 2θ of 4.85° (d<sub>001</sub> = 1.82 nm) for the pillared sample dried at 100 °C. The peaks observed at 2θ of 4.85° and 3.17° resulted from the disordered structure while the third one corresponded to the 001 diffraction reflections. The intensity of the peak (which was caused by the delaminated structure) at 2θ of 3.17° was higher than the one that occurred at 2θ of 6.60°. This behaviour showed that synthesised Fe-PILC was mesoporous and had high surface area as concluded from the nitrogen adsorption/desorption isotherm (Figure 5). Upon calcination at 300 °C, shifts in 2θ values to the higher values occurred.

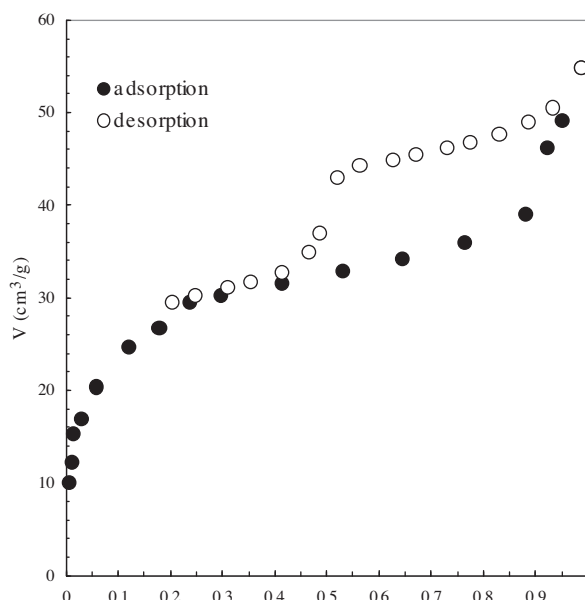


**Figure 5.** Nitrogen adsorption/desorption isotherm of Fe-PILC at 77 K.

**Surface acidity:** Acidity is one of the most important properties required for PILCs in addition to good textural properties. The surface acidities of the host and Fe-PILC were determined by volumetric titration and FTIR spectra of original, pyridine adsorbed/desorbed samples. FTIR spectra of HGB and PILC are given in 7 and FTIR spectra of samples recorded after pyridine desorption at room temperature, 150, 250, and 350 °C are given in Figure 8 to investigate the type of acid sites. The total surface acidity of Fe-PILC was measured as 127.93 meqv.(100 g)<sup>-1</sup> by titration (Table 3).

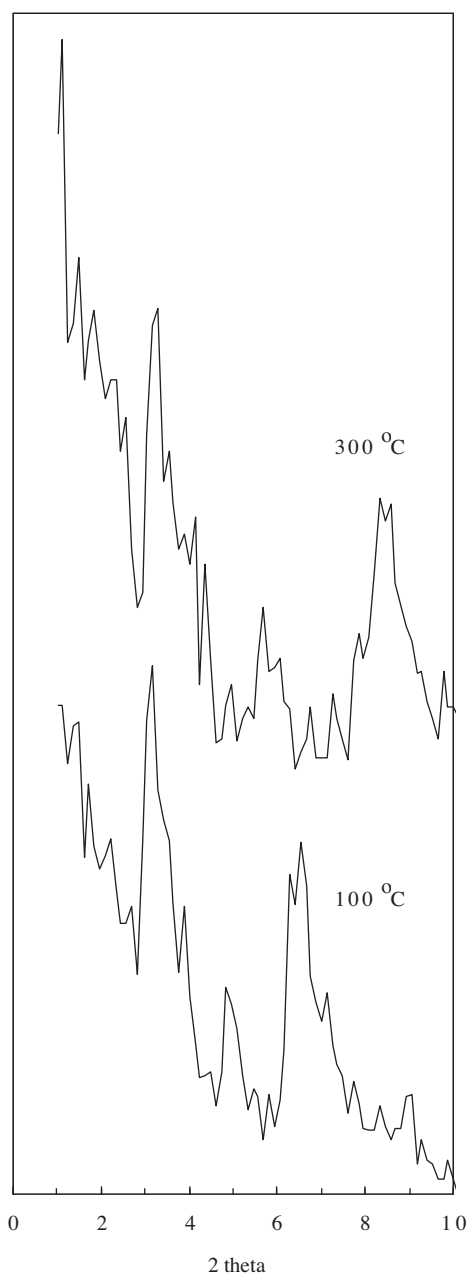


**Figure 6.** Small angle scattering XRD patterns of Fe-PILC at 100 and 300 °C.

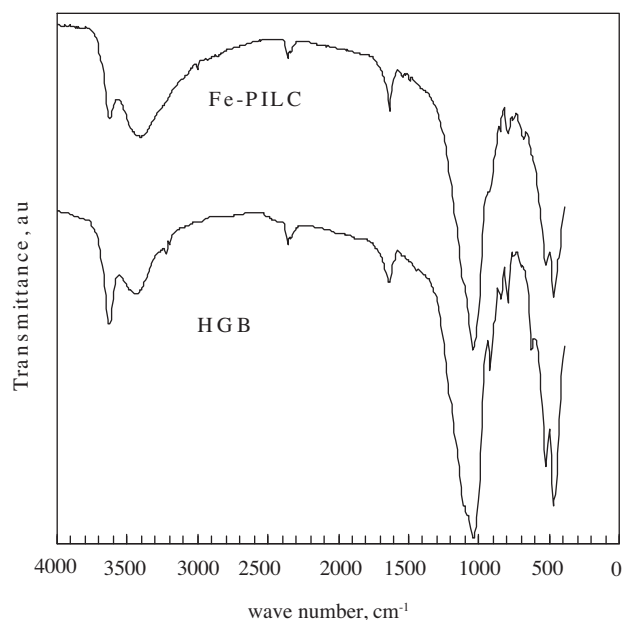


**Figure 7.** FTIR spectra of HGB and Fe-PILC samples.

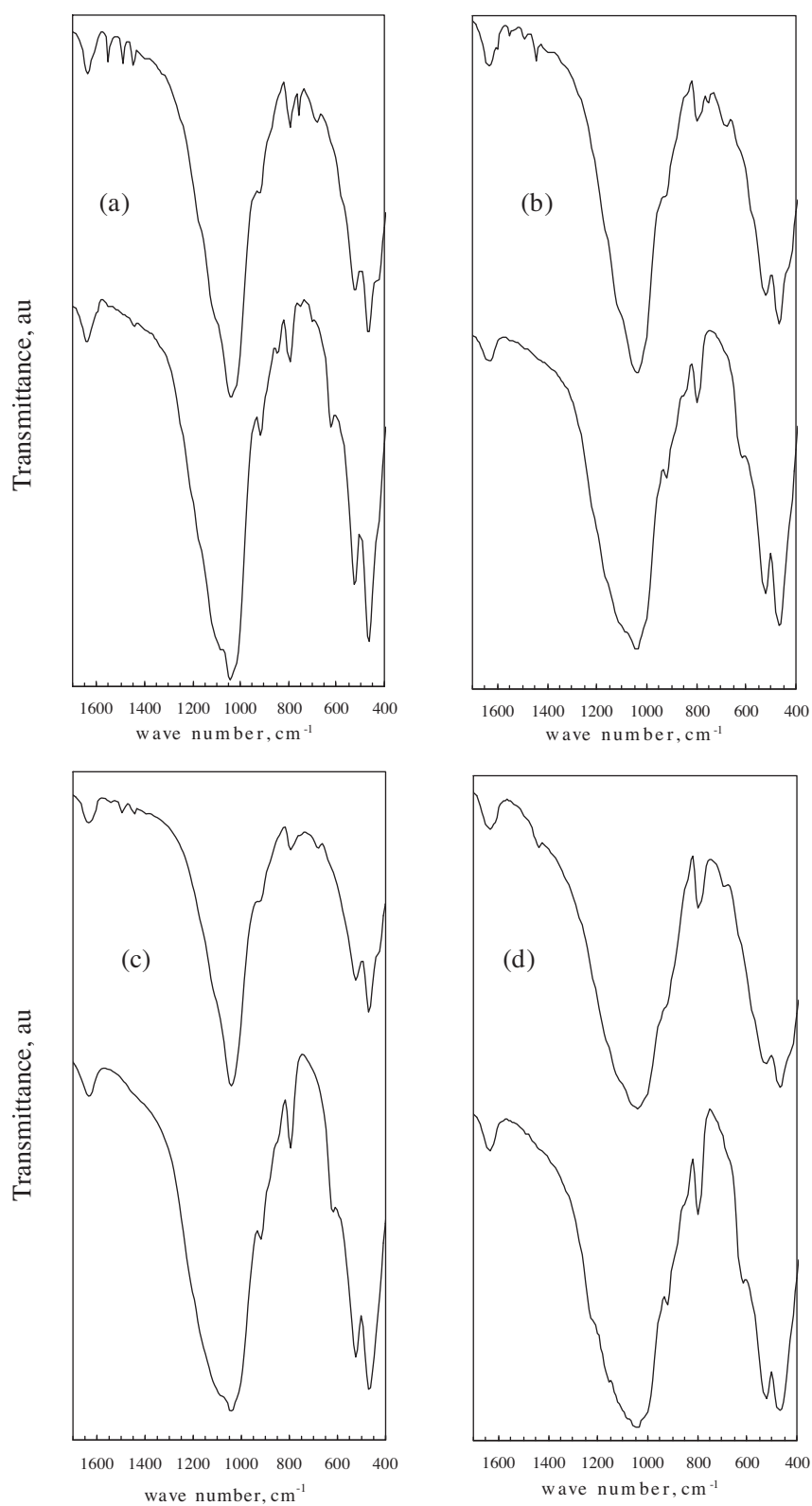


**Figure 8.** FTIR spectra of Fe-PILC and HGB samples at different pyridine desorption temperature (a) room temperature (b) 150 °C (c) 250 °C (d) 350 °C (from top to bottom Fe-PILC and HGB).

Small decreases in the peak intensities of the band at  $470\text{ cm}^{-1}$  corresponding to AlO stretching and a shift of Si-O-Si stretching vibration at  $1033\text{ cm}^{-1}$  towards slightly higher frequency were observed with pillaring (Figure 7). The bands at  $917\text{ cm}^{-1}$  (OH deformation linked to  $2\text{ Al}^{3+}$ ) and  $848\text{ cm}^{-1}$  (OH deformation linked to  $\text{Al}^{3+}$ ,  $\text{Mg}^{2+}$ ) decreased with pillaring. The intensity of the water bending vibration band that occurred at  $1635\text{ cm}^{-1}$  increased with intercalation. Pillaring also resulted in a small band at  $3000\text{ cm}^{-1}$  due to OH-stretching of bonded metal ions. The peak at  $3640\text{ cm}^{-1}$ , which was ascribed to the metal-OH stretching in the octahedral layer, decreased with pillaring, while the broad band at  $3440\text{ cm}^{-1}$  corresponding to interlayer/adsorbed water on the surface became dominant. The interlayer water band at  $3224\text{ cm}^{-1}$  completely disappeared with pillaring. The band at  $2380\text{ cm}^{-1}$  was assigned to carbonates or bicarbonates and did not change with pillaring.<sup>35–37</sup>

The FTIR spectra of samples of pyridine sorbed samples showed that the bands at  $1485\text{ cm}^{-1}$ ,  $1540\text{ cm}^{-1}$ ,  $1590\text{ cm}^{-1}$ , and  $1635\text{ cm}^{-1}$  corresponding to pyridinium cations and the bands at  $753\text{ cm}^{-1}$ ,  $1440\text{ cm}^{-1}$ ,  $1490\text{ cm}^{-1}$ , and  $1638\text{ cm}^{-1}$  indicating the presence of Brönsted acid sites became dominant with pillaring. The intense peak at  $1550\text{ cm}^{-1}$  due to Brönsted acidity was observed while it was absent for the original clay. The spectrum recorded after pyridine desorption at  $150\text{ }^{\circ}\text{C}$  showed the continued existence of both Lewis and Brönsted acidity. The peaks at  $1638\text{ cm}^{-1}$  and  $1440\text{ cm}^{-1}$  were still preserved while the intensity of band at  $1590\text{ cm}^{-1}$  (small shoulder) were decreased and the one that occurred at  $753\text{ cm}^{-1}$  disappeared at desorption temperatures higher than  $150\text{ }^{\circ}\text{C}$ . The peak intensity at  $1490\text{ cm}^{-1}$  common to both Lewis and Brönsted sites decreased with the increase in desorption temperature. The band at  $1635\text{ cm}^{-1}$  (small shoulder) became more diffuse at elevated desorption temperatures. It was concluded that Fe-PILC exposed a stronger intensity of bands corresponding to both acid sites (Figure 8).<sup>7,14,35–41</sup>

## Conclusions

Several Fe-PILCs synthesised from bentonite rock showed similar behaviours with the ones obtained from the SWy-2 (Wyoming) clay mineral. The findings were also in agreement with the literature studies.<sup>11–19,24,34–40</sup> The surface area values increased with increasing calcination temperature at moderate temperatures. At elevated temperatures decreases in surface area and basal spacing values were observed. Up to  $800\text{ }^{\circ}\text{C}$  calcination temperature, thermally stable porous products were obtained. Nitrogen adsorption/desorption isotherms showed hysteresis loops in the desorption branch indicating the presence of mesopores. The XRD analysis showed that delaminated Fe-PILC with d-spacing values up to  $2.79\text{ nm}$  was obtained. The results simply implied that the surface acidity of the clay was enhanced by pillaring. The PILC both had Brönsted and Lewis acid sites with dominant Brönsted acid site peaks. The bands corresponding to Lewis acid sites nearly disappeared while those corresponding to chemically sorbed pyridine were preserved at elevated desorption temperatures.

## Acknowledgements

This work was partially funded by the Scientific and Technological Research Council of Turkey, TÜBİTAK-MİSAG-60, TÜBİTAK-MİSAG 172, and by the Turkish State Planning Organisation Research Project of DPT/99K 120340.

### References

1. Barrer, R. M.; McLeod, D. M. *Trans. Faraday Soc.* **1955**, *51*, 1290-1300.
2. Figueras, F., *Catal. Rev. Sci. Eng.*, **1988**, *30*, 457-499.
3. Klotz, J. T. *J. Porous Mater.*, **1998**, *5*, 5-41.
4. Gil, A.; Gandia, L. M.; Vicente, M. A. *Catal. Rev., Sci. Eng.*, **2000**, *42*, 145-212.
5. Centi, G.; Perathoner, S. *Micropor. Mesopor. Mater.*, **2008**, *107*, 3-15.
6. Fetter, G.; Heredia, G.; Velazquez, L. A.; Maubert, A. M.; Bosch, P. *Appl. Catal. A-Gen.*, **1997**, *162*, 41-45.
7. Chae, H. J.; Nam, I. S., Ham, S. W.; Hong, S. B. *Catal. Today*, **2001**, *68*, 31-40.
8. Salerno, P.; Asenjo, M. B.; Mendioroz, S. *Thermochim Acta*, **2001**, *379*, 101-109.
9. Klotz, J. T.; Evans, R.; Hickey, L.; Frost, R. L. *Appl. Clay Sci.*, **2002**, *20*, 157-163.
10. Vicente, M. A.; Belver, C.; Trujillano, R.; Rives, V.; Alvarez, A. C.; Lambert, J. F.; Korili, S. A.; Gandia, L. M.; Gil, A. *Appl. Catal. A-Gen.*, **2004**, *267*, 47-58.
11. Chen, J. P.; Hausladen, M. C.; Yang, R. T. *J. Catal.*, **1995**, *151*, 135-146.
12. Zurita, M. J. P.; Vitale, G.; Goldwasser, M. R. *J. Molecular Catal. A: Chem.*, **1996**, *107*, 175-183.
13. Choudary, B. M.; Kantam, M. L.; Sateesh, M.; Rao, K. K. *Appl. Catal. A: Gen.*, **1997**, *149*, 257-264.
14. He, N.; Bao, S.; Xu, Q. *Appl. Catal. A: Gen.*, **1998**, *169*, 29-36.
15. Letaief, S.; Casal, B.; Aranda, P.; Martin-Luengo, M. A.; Ruiz-Hitzky, E. *Appl. Clay Sci.*, **2003**, *22*, 263-277.
16. Belkhadem, F.; Clacens, J. M.; Bengueddach, A.; Figueras, F. *Appl. Catal. A: Gen.*, **2006**, *298*, 188-193.
17. Ksontini, N.; Najjar, W.; Ghorbel, A. *J. Phys. Chem. Solids*, **2008**, *69*, 1112-1115.
18. Mandalia, T.; Crespin, M.; Messad, D.; Bergaya, F. *Chem. Commun.* **1998**, 2111-2112.
19. Yuan, P.; Bergaya, F. A.; Tao, Q.; Fan, M.; Liu, Z.; Zhu, J.; He, H., Chen, T. *J. Colloid Inter. Sci.*, **2008**, *324*, 142-149.
20. Huerta, L.; Meyer, A.; Choren, E. *Micropor. Mesopor. Mater.*, **2003**, *57*, 219-227.
21. Belaroui, L. S.; Millet, J. M. M.; Bengueddach, A. *Catal. Today*, **2004**, *89*, 279-287.
22. Belver, C.; Banares-Munoz, M. A.; Vicente, M. A. *Appl. Catal. B-Environ.*, **2004**, *50*, 101-112.
23. Yuan, P.; He, H.; Bergaya, F.; Wu, D.; Zhou, Q.; Zhu, J. *Micropor. Mesopor. Mater.*, **2006**, *88*, 8-15.
24. Balci, S.; Gökçay, E. *Mater. Chem. Phys.*, **2002**, *76*, 46-51.
25. Maes, N.; Vansant, E. T. *Microporous Mater.* **1995**, *4*, 43-52.
26. Bain, D. C.; Smith, B. F. L., in Wilson, M. J. (Ed.) *Chemical analysis, in Clay mineralogy: spectroscopic and chemical determinative methods* Chapman & Hall Co., **1994**, pp. 300-332.
27. Kumar, P.; Jasra, R. V.; Bhat, T. S. G. *Ind. Eng. Chem. Res.*, **1995**, *34*, 1440-1448.
28. Tomul, F., Balci, S. *Appl. Clay Sci.*, **2009**, *43*, 13-20.
29. Tomul, F., Balci, S. *G. U. J. Sci.*, **2008**, *21*, 21-31.
30. Brindley, G. W. in Brindley, G. W.; Brown, G. (Eds.) *Crystal structure of clay minerals and their X-Ray identifications* Monograph 5, Mineralogical Society, **1980**, pp. 411-438.

31. Brown, G.; Brindley, G. W. in Brindley, G. W.; Brown, G. (Eds.) Crystal structure of clay minerals and their X-Ray identifications Monograph 5, Mineralogical Society, **1980**, pp. 305-360.
32. Balcı, S.; Gökçay, E. Nanoparticles, Nanostructures & Nanocomposites Conf., **2004**, pp.121.
33. Altın, O.; Özbelge, Ö. H.; Doğu, T. *J. Colloid Inter. Sci.*, **1998**, 198, 130-140.
34. Rauquerol, F.; Rouquerol, J.; Sing, K. Adsorption by Powders & Porous Solids Academic Press, London, **1999**, pp. 165-234.
35. Auer, H.; Hofmann, H. *Appl. Catal. A-Gen.*, **1993**, 97, 23-38.
36. Storaro, L.; Lenarda, M.; Ganzerla, R.; Rinaldi, A. *Micropor. Mater.*, **1996** 6, 55-63.
37. Kurian, M.; Sugunan, S. *Micropor. Micropor. Mater.*, **2005**, 83, 25-34.
38. Occellia, M. L.; Biza, S.; Auroux, A.; Iyer, P. S. *App. Catal. A. Gen.*, **1999**, 179, 117-129.
39. Breen, C.; Deane, A. T.; Flynn, J. J. *Clay Miner.*, **1987**, 22, 169-178.
40. Belkhadem, F.; Maldonado, A.; Siebenhaar, B.; Clacens, J. M.; Perez Zurita, M. J.; Bengueddach, A.; Figueras, F. *App. Clay Sci.*, **2008**, 39, 28-37.
41. Moronta, A.; Oberto, T.; Carruyo, G.; Solano, R.; Sanchez, J.; Gonzalez, E.; Huerta, L. *App. Catal. A. Gen.*, **2008**, 334, 173-178.